

Disentangled Representation Learning for RF Fingerprint Extraction under Unknown Channel Statistics

Renjie Xie, Wei Xu, *Senior Member, IEEE*, Jiabao Yu,
Aiqun Hu, *Senior Member, IEEE*, Derrick Wing Kwan Ng, *Fellow, IEEE*,
and A. Lee Swindlehurst, *Fellow, IEEE*

Abstract

Deep learning (DL) applied to a device's radio-frequency fingerprint (RFF) has attracted significant attention in physical-layer authentications due to its extraordinary classification performance. Conventional DL-RFF techniques, trained by adopting maximum likelihood estimation (MLE), tend to overfit the channel statistics embedded in the training dataset. This restricts their practical applications as it is challenging to collect sufficient training data capturing the characteristics of all possible wireless channel environments. To address this challenge, we propose a DL framework of disentangled representation learning (DRL) that first learns to factor the input signals into a device-relevant component and a device-irrelevant component via adversarial learning. Then, it synthesizes a set of augmented signals by shuffling these two parts within a given training dataset for training of subsequent RFF extractor. The implicit data augmentation in the proposed framework imposes a regularization on the RFF extractor to avoid the possible overfitting of device-irrelevant channel statistics, without collecting additional data from unknown channels. Experiments validate that the proposed approach, referred to as DR-RFF, outperforms conventional methods in terms of generalizability to unknown complicated propagation environments, e.g., dispersive multipath fading channels, even though all the training data are collected in a simple environment with dominated direct line-of-sight (LoS) propagation paths.

Index Terms

Physical layer authentication, open set, radio frequency fingerprint (RFF), adversarial training, self-supervised learning, disentangled representation, metric learning, data augmentation.

R. Xie, W. Xu, J. Y. and A. Hu are with the National Mobile Communications Research Laboratory, Southeast University, Nanjing 210096, China (e-mail: renjie_xie@seu.edu.cn, wxu@seu.edu.cn, yujiabao@seu.edu.cn, aqhu@seu.edu.cn).

D. W. K. Ng is with the School of Electrical Engineering and Telecommunications, University of New South Wales, Sydney, NSW 2052, Australia (e-mail: w.k.ng@unsw.edu.au).

A. L. Swindlehurst is with the Center for Pervasive Communications and Computing, University of California, Irvine, CA 92697-2625 USA (e-mail: swindle@uci.edu).

I. INTRODUCTION

State-of-the-art authentication using inherent physical-layer characteristics has shown great potential in securing communication in the future Internet-of-Things (IoT) networks [1]. Compared to conventional higher-layer authentication techniques, physical-layer authentication (PLA) exploits inherent hardware unique characteristics of individual terminal devices, known as their radio-frequency fingerprint (RFF), to perform effective authentication. Analogous to human fingerprints, these hardware characteristics are naturally caused by manufacturing deviations and are difficult to modify or tamper with [2]. Authentication with RFF has the advantages of short latency, low power consumption, and marginal computational overhead, which is appealing for practical implementations [3].

To enable RFF authentication, it is essential to extract discriminative RFFs from the signals sent by the desired devices, and as a result, intensive efforts have been devoted to extracting stable RFFs. Conventionally, handcrafted features based on expert knowledge have been adopted to extract the RFFs [4]–[6]. However, due to the limitations of expert knowledge to the nonlinear hardware characteristics, these handcrafted features usually suffer from low discrimination ability, and cannot cope with the growing IoT applications with massive numbers of devices [7].

Deep learning (DL)-based methods with their learning capability have recently been exploited for effective nonlinear feature extraction in physical-layer applications [8]–[10], especially for RFF extraction. For instance, in [11], [12], the authors extracted the RFFs using a convolutional neural network (CNN), a popular type of deep neural network (DNN). In our previous work [13], a softmax-based metric learning approach was adopted for enabling device authentication by strengthening the generalizability of the DL-based RFFs, such that unknown devices can be recognized even with the existence of unknown device aging. Similarly, in [14], a metric learning approach based on triplet loss was proposed to enable unknown device authentication. Thanks to the ability of DNNs to learn the RFF features themselves, the classification performance of these DL-based RFFs is noticeably better than that obtained with handcrafted RFFs.

Despite these promising improvements, the above mentioned DL-based methods, e.g., [11]–[13], are typically trained as a maximum-likelihood (ML) estimator. In particular, their performance heavily relies on the quality of the collected training data. In practice, the training data collected for the RFF extraction inevitably contains both hardware characteristics and the impacts of the propagation environment. On the other hand, the DL-based RFFs trained using data from

channels under a specific propagation environment, e.g., line-of-sight (LoS)-dominated channels, tend to overfit the resulting model. More importantly, the methods sometimes fail to generalize the results to other types of channels such as those with considerable multipath. Unfortunately, this challenge cannot simply be addressed by collecting more training data that covers all possible wireless channel environments. In real-world IoT networks, collecting data representative of all possible channel conditions is prohibitively expensive if not impossible. One possible approach for avoiding this overfitting in the DL-based RFFs is to apply data augmentation (DA) techniques for training the RFF extractor [14]–[16]. Despite certain improvements, DA-based methods still heavily rely on the specific channel models as prior knowledge. In particular, if there is a mismatch between the channel models adopted in DA and those encountered in the field, the improvement achieved by DA would diminish which in turn degrades the RFF authentication.

In this paper, we propose a novel framework based on disentangled representation learning (DRL) [17] to improve the generalizability of DL-based RFFs to unknown and complicated channel statistics. DRL techniques [18]–[20] have been targeted for applications in wireless communication, including but not limited to indoor localization [21], joint source coding [22], [23], as well as unsupervised RF fingerprinting [24]. In general, these methods learn input-to-latent-variable mapping based on the assumption of a prior distribution over the latent space. Since the learning of these frameworks is unsupervised, the semantic information contained in each dimension of the latent space is uncontrollable and uncertain. Unlike these conventional DRL techniques, the proposed DRL framework aims at separating the input signal into two disjoint parts with certain meanings. The main contributions of this work are threefold.

- 1) We propose to factor the received signal into *device-relevant* and *device-irrelevant* representations via two DNNs. The device-relevant representation refers to the essential information for effective RFF and the device-irrelevant representation represents the “background” of the signal, which contains both noise and the effects of RF propagation. A domain-preserving network is proposed for generating augmented signals using these two representations. To achieve this factorization, we design specific self-supervised learning criteria that adversarially suppress the device-relevant information in the “background.”

- 2) We exploit the fact that even though the devices may be located in similar environments or nearby each other, distinctions in the “background” of the received signals will still exist. Based on this observation, the proposed DRL framework shuffles the “backgrounds” within the original training data, which implicitly synthesizes more data and maximally enlarges the data

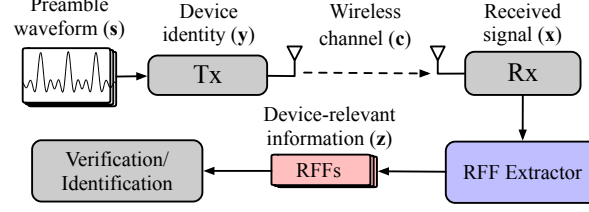


Fig. 1. The diagram of a RFF authentication system.

space in a data-driven manner.

3) We evaluate the proposed methods using a real-world testbed. The experiments verify that the proposed DRL framework outperforms conventional DL-RFFs for unknown channels. The implicit data augmentation in the proposed DRL framework can significantly reduce the overfitting of known channels and provide a better trade-off between robustness and performance than the conventional methods.

The rest of this paper is organized as follows. Section II describes the system model. Section III elaborates the details of the proposed method, and Section VI presents the experimental tests and results. Finally, Section V concludes this paper.

Notation: Throughout this paper, boldface lower case letters denote a random column vector, \mathbf{a}^\top and $\|\mathbf{a}\|$ denote the transpose and the l_2 -norm of vector \mathbf{a} , $\mathcal{I}(\mathbf{a}; \mathbf{b})$ denotes the mutual information between \mathbf{a} and \mathbf{b} , $(\mathbf{x}_i, \mathbf{y}_i)$ denotes the i -th sample from a dataset, $\mathcal{N}(\mathbf{0}, \mathbf{I})$ denotes the real-valued normal distribution with zero mean and identity covariance, the operator $[\cdot]_+$ is defined as $[\cdot]_+ \triangleq \max\{\cdot, 0\}$ and $\nabla_A(\mathcal{L})$ represents the gradient of \mathcal{L} with respect to the trainable parameters of the DNN module A .

II. SYSTEM OVERVIEW

A. Open-set RFF Authentication

We consider an RFF authentication system as depicted in Fig. 1 that consists of K transmitting terminals and one server. Formally, given a preamble of length M , denoted by $\mathbf{s} \in \mathbb{C}^M$, the received signals $\mathbf{x} \in \mathbb{C}^M$ can be written as

$$\mathbf{x} = f_c(f_y(\mathbf{s})), \quad (1)$$

where $f_c : \mathbb{C}^M \rightarrow \mathbb{C}^M$ is the functional representation of the wireless channel and $f_y : \mathbb{C}^M \rightarrow \mathbb{C}^M$ represents the effects imposed by the hardware characteristics of the transmitter.

The identity of the transmitter is denoted as $\mathbf{y} \in \{\mathbf{y}_{(i)} : i = 1, \dots, K\}$ where $\mathbf{y}_{(i)}$ is a vector with an “1” in position i and zeros elsewhere, indicating which of the K legitimate terminals the signal corresponds to. The authentication system uses the RFF extractor to separate the inherent hardware characteristics from the received signal \mathbf{x} , i.e., the RFF. Mathematically, we denote this by

$$\mathbf{z} = F(\mathbf{x}), \quad (2)$$

where $F : \mathbb{C}^M \rightarrow \mathbb{R}^d$ is the RFF extractor implemented using some type of DNN. The obtained RFF \mathbf{z} of length d is then compared against known RFFs using some distance function in the final step of the device authentication process. In particular, given a distance function $D(\cdot, \cdot)$, verification of RFF \mathbf{z}_i against RFF \mathbf{z}_j can be achieved as follows,

$$\begin{cases} D(\mathbf{z}_i; \mathbf{z}_j) \leq T & \Rightarrow \mathbf{y}_i = \mathbf{y}_j, \\ D(\mathbf{z}_i; \mathbf{z}_j) > T & \Rightarrow \mathbf{y}_i \neq \mathbf{y}_j, \end{cases} \quad (3)$$

where T is a threshold that is to be optimized based on the given training data. In this work, we adopt cosine distance $D(\mathbf{z}_i; \mathbf{z}_j) = 1 - \cos(\mathbf{z}_i, \mathbf{z}_j)$ as the distance function. To achieve satisfactory authentication performance, the RFF \mathbf{z} should not only be sufficiently discriminative, but the value of \mathbf{z} should only depend on the hardware properties encoded by $f_{\mathbf{y}}(\cdot)$. In other words, this requires the RFF extractor $F(\cdot)$ to maximally mitigate the impact of the wireless channels, i.e., $f_{\mathbf{c}}(\cdot)$, while retaining the unique characteristics of the device hardware.

B. ML RFF Extractor

In order to retain device-relevant information and to obtain discriminative RFFs, a maximum likelihood (ML) RFF extractor was previously proposed in [13]. Given a training set $\mathcal{T} = \{(\mathbf{x}_i, \mathbf{y}_i)\}_{i=1}^N$ with N samples, the ML RFF extractor $F(\cdot)$ in [13] is obtained by solving the optimization problem:

$$\max_{F, \mathbf{W}} \quad \frac{1}{N} \sum_{i=1}^N \ln p_{\mathbf{W}}(\mathbf{y}_i | \mathbf{z}_i), \quad \text{s.t.} \quad \mathbf{z}_i = F(\mathbf{x}_i), \quad (4)$$

where $p_{\mathbf{W}}(\mathbf{y} | \mathbf{z})$ is an auxiliary classifier that establishes the relationship between RFF \mathbf{z} , and the device identity \mathbf{y} . \mathbf{W} is a set of trainable parameters in the auxiliary classifier.

Hypersphere projection: To achieve device discrimination with \mathbf{z} , $p_{\mathbf{W}}(\mathbf{y} | \mathbf{z})$ is implemented

in the form of a softmax probability [25]:

$$p_{\mathbf{W}}(\mathbf{y}_{(i)}|\mathbf{z}) = \frac{\exp\{\bar{\mathbf{w}}_i^\top \bar{\mathbf{z}}\}}{\sum_j \exp\{\bar{\mathbf{w}}_j^\top \bar{\mathbf{z}}\}}, \quad \forall i = 1, 2, \dots, K, \quad (5)$$

where we define

$$\bar{\mathbf{w}} = \frac{\mathbf{w}}{\|\mathbf{w}\|} \quad \text{and} \quad \bar{\mathbf{z}} = \delta \frac{\mathbf{z}}{\|\mathbf{z}\|}, \quad (6)$$

and $\delta > 0$ is a hyper-parameter that controls the norm of $\bar{\mathbf{z}}$. Here, $\mathbf{W} = \{\{\mathbf{w}_j\}_{j=1}^K\}$ represents the parameters of the softmax classifier. The normalization in (6) is also known as hypersphere projection (HP), where δ is the radius of the hypersphere. Note that HP is popularly adopted in facial recognition [25]–[27], and it regulates the norms of the feature vector to guarantee that (4) is equivalent to using the cosine distance to perform discrimination of the RFFs. Using this formulation, the RFF extractor $F(\cdot)$ can maximally retain the device-relevant information in \mathbf{x} to improve the quality of the RFF discrimination.

Given sufficient training data representative of the entire data space of channel realizations, the ML RFF extractor is the best in the sense of probability of successful RFF discrimination [28]. However, collecting sufficient data to capture the entire dynamic channel space in real-world scenarios is expensive and impractical, especially for massive IoT applications. If the training data is insufficiently rich, e.g., if it is collected only from simple LoS-dominated channels, the ML RFF extractor will tend to overfit this non-representative channel statistic presented in the training data. More importantly, generalizations of this approach to other types of channels, e.g., dispersive multipath channels, is limited.

III. DISENTANGLED REPRESENTATION LEARNING FOR RFF EXTRACTION

In this section, we propose a DRL framework to improve the generalizability of DL-RFFs adapting to practical wireless channels drawn from distributions that are unavailable or unseen in the training data. We first introduce the main idea of the design and then elaborate on the details of the proposed DRL framework.

A. Proposed DRL Framework

Representation learning (RL) is a set of techniques that learn to extract representations from raw data for facilitating downstream tasks [29]. It aims to automatically project high-dimensional real-world sensory data into a low-dimensional space to extract semantic information that is

more mathematically or computationally convenient to process. One important branch of the RL techniques, namely disentangled representation learning (DRL), involves not only projecting the observed data onto a lower dimension form, but also breaking down or disentangling the data into meaningful underlying factors for subsequent data reconstruction [17], [30]. Several interesting applications have been explored based on this unique disentangling capability. For example, in video prediction, DRL was exploited to disentangle moving objects in a surveillance video from static background [31], [32]. Also, the DRL in [33] was used to disentangle speech signals into speaker identities and speaking styles, accents, and emotions associated with the speech signals. Furthermore, the DRL in [34] extracted pose information and facial identities of from images to synthesize identity-preserving faces and achieve pose-invariant facial recognition. Indeed, with an appropriate DRL design, one can obtain deep models that are robust to representations from unseen domains that conventional DA techniques cannot always achieve, e.g., [34]–[36]. In the context of RFF extraction, the main task of our proposed DRL framework is to adversarially learn to extract the discriminative RFFs from the received signals, while provide robustness against the type of underlying wireless channel.

The proposed DRL framework first learns to factor the received signal into two disjoint parts, i.e., a *device-relevant* representation and a *device-irrelevant* representation, and then to synthesize augmented training signals given these representations. Here, the *device-relevant* representations are the RFFs and the *device-irrelevant* representations are regarded as other “background” information associated with the received signals such as that associated with the propagation environment. This ability of the DRL framework allows us to swap the backgrounds of different signals and thus create new data for augmenting the training set.

In practice, due to slight differences in the angle and position of the device antennas when acquiring signals, even if the training data from all the devices are collected in a simple LoS scenario, distinctions between their channels can still exist. Thus, the training dataset may still contain multiple different backgrounds among its various signals. By disentangling the signals into device identities and backgrounds, we can generate augmented signals that preserve device identity and that are representative of data that would be generated by the device under every possible background in the training dataset. Since the background distinctions are essentially distinction in the channels, the RFF extractors trained by these augmented signals are encouraged to ignore these channel distinctions and extract channel-invariant features based solely on the RFFs

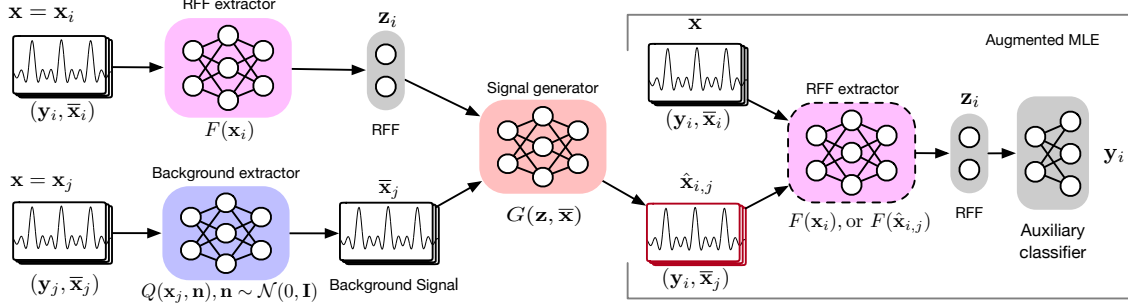


Fig. 2. The proposed DRL framework for RFF extraction (**F-step**). Given the two received training signals, the RFF and the background signal are extracted by the RFF extractor (pink) and the background extractor (blue), respectively. A synthetic signal is generated by feeding the RFF and the background signal to the signal generator (red). The raw and synthetic signals, which have the same RFF but different signal backgrounds, are used to train the RFF extractor (pink dotted box).

It should be noted that the proposed DRL framework can be realized via semi-supervising learning [37], e.g., using a small number of devices to collect various channel conditions to provide background information. In this paper, we consider the simple approach of collecting the training dataset under only simple LoS scenarios. A promising observation from our experiments in Section IV is that the channel variations under the LoS assumption are sufficiently rich to improve the generalizability of the RFF extractor in the test sets. The proposed framework, as depicted in Fig. 2, consists of three main DNN modules, i.e., $F(\cdot)$, $Q(\cdot, \mathbf{n})$, and $G(\cdot, \cdot)$. We articulate these three modules below.

a) **RFF extractor** $F(\cdot)$: This module, represented by the pink boxes in Fig. 2, takes signal \mathbf{x} as the input and outputs the corresponding RFF \mathbf{z} in (2). The vector \mathbf{z} is taken to be the device-relevant information within \mathbf{x} . Besides its uses as an RFF extractor, this module is also adopted as an adversarial discriminator for estimating how much of the device-relevant information is contained in the background signal from $Q(\cdot, \mathbf{n})$, which is introduced next.

b) **Background extractor** $Q(\cdot, \mathbf{n})$: This module, shown as the blue box in Fig. 2, realizes a stochastic mapping which is used for preserving device-irrelevant information while ruling out device-relevant information as much as possible. Given the input signal \mathbf{x} , the background signal, denoted by $\bar{\mathbf{x}}$, is obtained as

$$\bar{\mathbf{x}} \sim p_Q(\bar{\mathbf{x}}|\mathbf{x}) \iff \bar{\mathbf{x}} = Q(\mathbf{x}, \mathbf{n}), \quad \mathbf{n} \sim \mathcal{N}(\mathbf{0}, \mathbf{I}). \quad (7)$$

This stochastic mapping is also used for sensitive information obfuscation in [38]. Similarly, the randomness in (7) is introduced for purposefully obfuscating the device-relevant information of \mathbf{x} . The background signal $\bar{\mathbf{x}}$, complementary to the RFF in forming \mathbf{x} , contains only the device-

irrelevant information within \mathbf{x} , which can capture the joint effects of the wireless channel, noise, the preamble waveform, etc.

c) Signal generator $G(\cdot, \cdot)$: This module, the centre red box in Fig. 2, is adopted for signal reconstruction and generation. The input to this module includes both the RFF and the background signal. Given these mutually complementary representations, the synthetic signal, denoted by $\hat{\mathbf{x}}$, is generated by

$$\hat{\mathbf{x}} = G(\mathbf{z}, \bar{\mathbf{x}}). \quad (8)$$

With these three modules, the proposed DRL framework establishes an efficient approach to generate augmented signals for improving the robustness of the RFF extraction. Ideally, exponentially more augmented data can be arbitrarily generated from the raw training set arbitrarily by swapping their background signals and introducing randomness. The training in our framework is performed in an iterative manner by the modules. Moreover, by applying the proposed framework, the augmented signals are also dynamically improved during the learning process. Details on the learning algorithm will be introduced later in Section III.E.

Note that the RFF extractor trained within the proposed framework is forced to extract the background-irrelevant (i.e., device-relevant) RFF information from the signals and therefore improve its generalizability and robustness. In the following, we refer to this RFF extractor as the *DR-RFF extractor*.

From the above, we see that $\bar{\mathbf{x}}$ and $\hat{\mathbf{x}}$ can both be adopted to extract the RFFs via $F(\cdot)$. Thus, in order to preserve the inference capability of $F(\cdot)$ for $\bar{\mathbf{x}}$ and $\hat{\mathbf{x}}$, we must restrict $G(\cdot, \cdot)$ and $Q(\cdot, \mathbf{n})$ to be domain-preserving [38], e.g., signal-to-signal transformations. The design of the learning procedure and the detailed structures of each of the three modules, i.e., $F(\cdot)$, $Q(\cdot, \mathbf{n})$, and $G(\cdot, \cdot)$, are elaborated in the following.

B. Learning DR-RFF Extractor $F(\cdot)$

Given the raw data pair in the training set, $(\mathbf{x}, \mathbf{y}) \in \mathcal{T}$, the augmented signals, $\hat{\mathbf{x}}$, are generated by the proposed DRL framework and $\hat{\mathbf{x}}$ contains the same device identity information but a different signal background compared to \mathbf{x} . The goal of the proposed DR-RFF extractor is to distill the same device-relevant information from both \mathbf{x} and $\hat{\mathbf{x}}$ while mitigating the impact of their backgrounds. From the perspective of information theory, this goal can be achieved by

maximizing the mutual information [39] between the corresponding RFFs and the device identity \mathbf{y} , as follows:

$$\max_F \quad \lambda \mathcal{I}(\mathbf{y}; \mathbf{z}) + (1 - \lambda) \mathcal{I}(\mathbf{y}; \hat{\mathbf{z}}) \quad \text{s.t.} \quad \mathbf{z} = F(\mathbf{x}), \quad \hat{\mathbf{z}} = F(\hat{\mathbf{x}}), \quad (9)$$

where $0 \leq \lambda < 1$ is a hyper-parameter that balances the learning effects for the raw and augmented signals. The first term in the objective function of (9), measuring the amount of device-relevant information extracted from the raw signal, is the same RFF learning objective as the one in our previous work [13]. The second term is the objective corresponding to the proposed augmented training. It encourages the RFF extractor $F(\cdot)$ to extract the same identity from the raw and augmented signals, which is the key to avoid overfitting of $F(\cdot)$ to the specific channel statistics embedded in the raw data.

To facilitate the applications of DNNs to solve the problem in (9), we now re-formulate it to obtain a tractable data-driven objective function. Mathematically, as exemplified in Fig. 2, we draw two arbitrary signals from devices \mathbf{y}_i and \mathbf{y}_j , collected under different propagation environments in the training dataset, i.e.,

$$(\mathbf{x}_i, \mathbf{y}_i) \in \mathcal{T}, \quad (\mathbf{x}_j, \mathbf{y}_j) \in \mathcal{T}. \quad (10)$$

From the left hand side of Fig. 2, the device-relevant RFF and the device-irrelevant background representations are respectively extracted as

$$\mathbf{z}_i = F(\mathbf{x}_i), \quad \bar{\mathbf{x}}_j = Q(\mathbf{x}_j, \mathbf{n}), \quad \text{for } \mathbf{n} \sim \mathcal{N}(\mathbf{0}, \mathbf{I}). \quad (11)$$

The synthetic signal, $\hat{\mathbf{x}}_{i,j}$, is generated from the above two representations via the signal generator as

$$\hat{\mathbf{x}}_{i,j} = G(\mathbf{z}_i, \bar{\mathbf{x}}_j), \quad (12)$$

where $\hat{\mathbf{x}}_{i,j}$ represents a received signal that is transmitted by device \mathbf{y}_i but undergoes the same propagation channel as device \mathbf{y}_j . In principle, the module $G(\cdot, \cdot)$ learns to mimic a transmission from device \mathbf{y}_i under the propagation environment of another device \mathbf{y}_j .

Following the derivations in [40] and [13], we reformulate (9) into an ML estimation as in

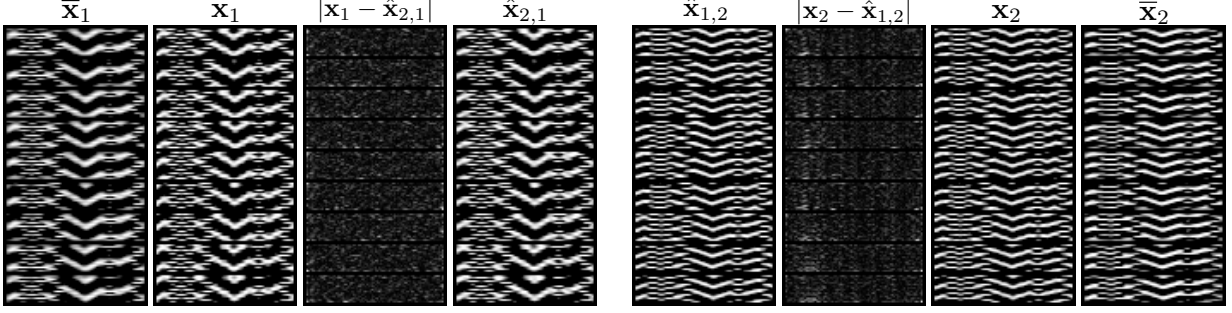


Fig. 3. Visualization of raw signals (\mathbf{x}_1 and \mathbf{x}_2), background signals ($\bar{\mathbf{x}}_1$ and $\bar{\mathbf{x}}_2$), and synthetic signals ($\hat{\mathbf{x}}_{1,2}$ and $\hat{\mathbf{x}}_{2,1}$).

(4). The learning problem for $F(\cdot)$ in (9), denoted by \mathcal{L}_F , is rewritten as

$$\mathcal{L}_F \triangleq \frac{1}{N^2} \sum_{i=1}^N \sum_{j=1}^N \left[\lambda \ln p_{\mathbf{W}}(\mathbf{y}_i | F(\mathbf{x}_i)) + (1 - \lambda) \ln p_{\mathbf{W}}(\mathbf{y}_i | F(\hat{\mathbf{x}}_{i,j})) \right]. \quad (13)$$

It is proved in [13] that $-\mathcal{L}_F$ is essentially a variational lower bound of (9). Learning this objective is equivalent to optimizing the original problem in (9) while circumventing the intractable computation in (9). The value of \mathcal{L}_F can be easily calculated using data samples. Thus, we can optimize the DR-RFF extractor $F(\cdot)$ using (13) and the gradient descent algorithm, e.g., Adam [41], with the training data set. Note that we detach every augmented signal $\hat{\mathbf{x}}_{i,j}$ from the generation process and treat it as an independent sample in training $F(\cdot)$. Therefore, we do not backtrack to the representation extraction when the back-propagation goes through the computational graph during the training of $F(\cdot)$.

One additional trick for the design of $F(\cdot)$ is that the HP operation in (6) applied to $p_{\mathbf{W}}(\mathbf{y}|\mathbf{z})$ is indispensable. For a successful disentanglement, the RFFs extracted by $F(\cdot)$ should contain as little of the background information as possible. This means that \mathbf{z}_i and $\mathbf{z}_{i,j}$ should be close to each other in terms of the cosine distance adopted in (3). The HP operation is necessary for obtaining discriminative RFFs, which is the key for aggregating the RFFs from the same device (e.g., \mathbf{z}_i and $\mathbf{z}_{i,j}$) under the cosine distance.

To more intuitively explain the intrinsic mechanisms of the proposed DRL framework, we visualize the real part of the raw signals, background signals, and the synthetic signals in Fig. 3. Comparing the raw signals with the background signals, we find that the textures of the signal backgrounds are dominant in the augmented signals. The difference signals, i.e., $|\mathbf{x}_1 - \hat{\mathbf{x}}_{1,2}|$ and $|\mathbf{x}_2 - \hat{\mathbf{x}}_{2,1}|$ in Fig. 3, reveal the embedded RFFs in the augmented signals indicating the fact that the device-relevant information in the signals is imperceptible.

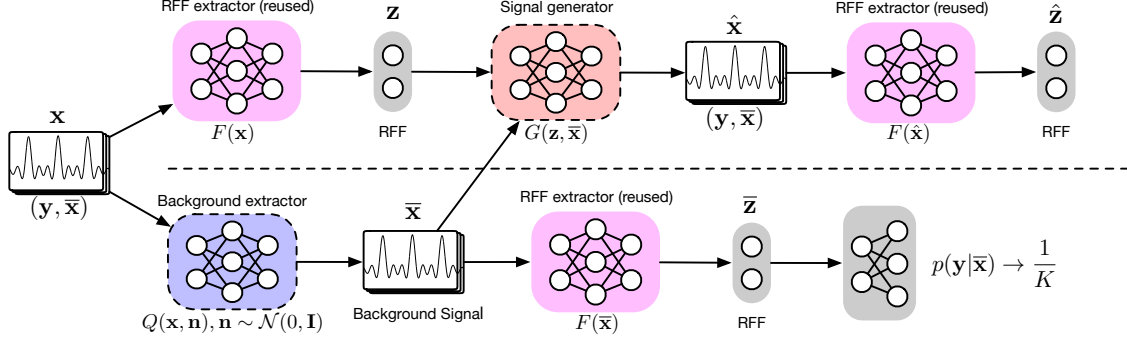


Fig. 4. The proposed DRL framework for RFF extraction (**Q/G-step**). Given a received signal, the background extractor (blue dotted box) learns to extract the background signal that cannot provide any discriminative ability to the fixed RFF extractor (pink). The signal generator (red dotted box) learns to reconstruct the signal by given RFF and the background signal. The reconstructed signal should also preserve the same RFF as the original signal.

C. Learning Background Extractor $Q(\cdot, \mathbf{n})$

The goal of $Q(\cdot, \mathbf{n})$ is to extract the background signals $\bar{\mathbf{x}}$ from the input signals \mathbf{x} . The background signal $\bar{\mathbf{x}}$ is expected to preserve as much information as possible from the inputs after removing the device-relevant information. Mathematically, this goal can be formulated as

$$\max_Q \mathcal{I}(\mathbf{x}; \bar{\mathbf{x}}), \quad \text{s.t.} \quad \mathcal{I}(\mathbf{y}; \bar{\mathbf{x}}) < \epsilon, \quad (14)$$

where $\mathcal{I}(\mathbf{x}; \bar{\mathbf{x}})$ and $\mathcal{I}(\mathbf{y}; \bar{\mathbf{x}})$ respectively quantify the amount of information that the background signal $\bar{\mathbf{x}}$ contains about that the original signal \mathbf{x} and the identity \mathbf{y} , and $\epsilon \geq 0$ is a hyper-parameter that controls the amount of device-relevant information that remains in $\bar{\mathbf{x}}$. To facilitate the subsequent development, we further relax the problem in (14) and convert it into an unconstrained problem by using a quadratic penalty [42] as follows:

$$\max_Q \mathcal{I}(\mathbf{x}; \bar{\mathbf{x}}) - \alpha [\mathcal{I}(\mathbf{y}; \bar{\mathbf{x}}) - \epsilon]_+^2, \quad (15)$$

where $\alpha > 0$ is the penalty parameter. The problem in (15) is equivalent to the original problem in (14) when $\alpha \rightarrow \infty$. This formulation is connected with the information bottleneck (IB) approach [43], which was initially designed for random variable compression and has been exploited for exploring the intrinsic learning mechanism of DNNs [44] and for training robust DNNs [40]. It is typically used for finding the best trade-off between model accuracy and representation complexity. In (14), we exploit this IB-like formulation to strike a balance between the “signal reconstruction quality” (i.e., the maximization of $\mathcal{I}(\mathbf{x}; \bar{\mathbf{x}})$) and the “elimination of device-relevant information” (i.e., the minimization of the penalty term) to achieve the disentanglement. In order

to facilitate the model training, we need to reformulate (15) by rewriting the learning objective with respect to only the training data. We rewrite the two terms in (15) into a data-driven form by respectively applying the techniques of *information maximization* [45] and *adversarial learning* [46], [47] as discussed in the following.

a) Information maximization: We begin with the calculation of the first term in (15). Due to the intractable conditional distribution $p(\mathbf{x}|\bar{\mathbf{x}})$, it is computationally expensive to directly calculate $\mathcal{I}(\mathbf{x}; \bar{\mathbf{x}})$. One common approach to address this problem is to adopt a tractable variational distribution $q(\mathbf{x}|\bar{\mathbf{x}})$ to replace $p(\mathbf{x}|\bar{\mathbf{x}})$. This replacement yields a tractable variational lower bound of $\mathcal{I}(\mathbf{x}; \bar{\mathbf{x}})$ which can be used for indirectly maximizing $\mathcal{I}(\mathbf{x}; \bar{\mathbf{x}})$. Following [45], we adopt the Gaussian distribution $q(\mathbf{x}|\bar{\mathbf{x}}) = \mathcal{N}(\mathbf{x}|\bar{\mathbf{x}}, \mathbf{I})$ to replace $p(\mathbf{x}|\bar{\mathbf{x}})$. The resultant variational lower bound, denoted by $-\mathcal{L}_v$, is

$$\begin{aligned}
& \max_Q \mathcal{I}(\mathbf{x}; \bar{\mathbf{x}}) \\
&= \max_Q \{h(\mathbf{x}) - h(\mathbf{x}|\bar{\mathbf{x}})\} \\
&= \max_Q \{h(\mathbf{x}) + \mathbb{E}_{p(\mathbf{x}, \bar{\mathbf{x}})}[\ln p(\mathbf{x}|\bar{\mathbf{x}})]\} \\
&\stackrel{(a)}{\geq} \max_Q \{h(\mathbf{x}) + \mathbb{E}_{p_Q(\bar{\mathbf{x}}|\mathbf{x})p(\mathbf{x})}[\ln \mathcal{N}(\mathbf{x}|\bar{\mathbf{x}}, \mathbf{I})]\} \\
&\stackrel{(b)}{\propto} \max_Q \left\{ \underbrace{-\mathbb{E}_{\mathbf{x} \in \mathcal{T}, \mathbf{n} \sim \mathcal{N}(\mathbf{0}, \mathbf{I})}[\|\mathbf{x} - Q(\mathbf{x}, \mathbf{n})\|^2]}_{-\mathcal{L}_v} + c \right\}, \tag{16}
\end{aligned}$$

where $h(\cdot)$ is the differential entropy [39], c is a constant that can be ignored, (a) follows by the nonnegativity of the Kullback-Leibler divergence (KLD), i.e.,

$$\mathcal{D}_{\text{KL}}(p(\mathbf{x}|\bar{\mathbf{x}}) \| q(\mathbf{x}|\bar{\mathbf{x}})) = \mathbb{E}_{p(\mathbf{x})} \left[\ln \frac{p(\mathbf{x}|\bar{\mathbf{x}})}{\mathcal{N}(\mathbf{x}|\bar{\mathbf{x}}, \mathbf{I})} \right] \geq 0, \tag{17}$$

and (b) follows by adopting the re-parameterization in (7) and dropping the constant terms that are irrelevant to $Q(\cdot, \mathbf{n})$. Therefore, the first term of (15) can be maximized by minimizing \mathcal{L}_v . With this new learning objective \mathcal{L}_v , the first term in (15) is simplified to a mean squared error (MSE) loss in (16), and hence the computational complexity of the optimization is greatly reduced.

b) Adversarial learning for the penalty: Similar to the first term, direct computation of the penalty $[\mathcal{I}(\mathbf{y}; \bar{\mathbf{x}}) - \epsilon]_+^2$ is intractable. The function of this term is to suppress any device-

relevant information. A variational approach like that used for $I(\mathbf{x}; \bar{\mathbf{x}})$ in (16) is not effective here since the MSE is not sensitive to the small differences in the device RFFs. Thus, we adopt the adversarial learning technique [46] to calculate this term. More concretely, as depicted in the lower half of Fig. 4, we reuse the DNN classifier, i.e., $p_{\mathbf{W}}(\mathbf{y}|F(\cdot))$ in Section III.B, as a discriminator to estimate the posterior $p(\mathbf{y}|\bar{\mathbf{x}})$, as follows:

$$\begin{aligned} \mathcal{I}(\mathbf{y}; \bar{\mathbf{x}}) &= \mathbb{E}_{p(\bar{\mathbf{x}})} [\mathcal{D}_{\text{KL}}(p(\mathbf{y}|\bar{\mathbf{x}}) \| p(\mathbf{y}))] \\ &\stackrel{(a)}{\approx} \mathbb{E}_{p(\bar{\mathbf{x}})} [\mathcal{D}_{\text{KL}}(p_{\mathbf{W}}(\mathbf{y}|F(\bar{\mathbf{x}})) \| p(\mathbf{y}))] \\ &\stackrel{(b)}{=} \mathbb{E}_{\bar{\mathbf{x}} \sim p_Q(\bar{\mathbf{x}}|\mathbf{x}), (\mathbf{x}, \mathbf{y}) \in \mathcal{T}} \left[\ln \frac{p_{\mathbf{W}}(\mathbf{y}|F(\bar{\mathbf{x}}))}{p(\mathbf{y})} \right], \end{aligned} \quad (18)$$

where (a) results from using the parameterized conditional distribution $p_{\mathbf{W}}(\mathbf{y}|F(\bar{\mathbf{x}}))$ to replace the original $p(\mathbf{y}|\bar{\mathbf{x}})$, and (b) follows by using the re-parameterization in (7), i.e., $\bar{\mathbf{x}} = Q(\mathbf{x}, \mathbf{n})$ for $\mathbf{n} \sim \mathcal{N}(\mathbf{0}, \mathbf{I})$. Here, the prior distribution of the identity \mathbf{y} can be taken to be a discrete uniform distribution, i.e., $p(\mathbf{y} = \mathbf{y}_{(i)}) = \frac{1}{K}, \forall i = 1, \dots, K$. Now, we can rewrite the penalty term in (15) in a data-driven form, denoted by \mathcal{L}_p , as follows

$$\mathcal{L}_p \triangleq - \left[\mathbb{E}_{\bar{\mathbf{x}} \sim p_Q(\bar{\mathbf{x}}|\mathbf{x}), (\mathbf{x}, \mathbf{y}) \in \mathcal{T}} \left[\ln \frac{p_{\mathbf{W}}(\mathbf{y}|F(\bar{\mathbf{x}}))}{1/K} \right] - \epsilon \right]_+^2. \quad (19)$$

Substituting (16) and (19) into (15), the learning objective of $Q(\cdot, \mathbf{n})$, denoted by \mathcal{L}_Q , is defined as

$$\mathcal{L}_Q \triangleq \mathcal{L}_v + \alpha \mathcal{L}_p. \quad (20)$$

Note that the value of \mathcal{L}_p depends on the RFF extractor $F(\cdot)$. In this sense, the learning of $Q(\cdot, \mathbf{n})$ can be treated as an adversarial game with two players: $Q(\cdot, \mathbf{n})$ tries to generate the signal to confuse $F(\cdot)$, while $F(\cdot)$, as the adversarial counterpart of $Q(\cdot, \mathbf{n})$, learns to discriminate the signals that are partially generated from $Q(\cdot, \mathbf{n})$.

D. Learning Signal Generator $G(\cdot, \cdot)$

The only remaining task is the development of the signal generator $G(\cdot, \cdot)$. As depicted in the upper half of Fig. 4, the module $G(\cdot, \cdot)$ takes a background signal, $\bar{\mathbf{x}}$, and the corresponding RFF, \mathbf{z} , as inputs for reconstructing the raw signal \mathbf{x} . The learning problem is designed as follows

$$\max_G \mathcal{I}(\mathbf{x}; \hat{\mathbf{x}}) + \beta \mathcal{I}(F(\mathbf{x}); F(\hat{\mathbf{x}})), \quad (21)$$

where $\hat{\mathbf{x}} = G(\mathbf{z}, \bar{\mathbf{x}})$, $\mathbf{z} = F(\mathbf{x})$, $\bar{\mathbf{x}}$ is drawn according to $p_Q(\bar{\mathbf{x}}|\mathbf{x})$, and $\beta > 0$ is a hyper-parameter that balances the two mutual information terms. In particular, the maximization of $\mathcal{I}(\mathbf{x}; \hat{\mathbf{x}})$ acts to minimize the signal reconstruction loss, which ensures the quality of the synthetic signal. The maximization of $\mathcal{I}(F(\mathbf{x}); F(\hat{\mathbf{x}}))$ ensures that the device-relevant information, i.e., the RFF, is successfully embedded in the synthetic signal.

Similar to the reformulation of (16), we adopt the variational approximation to solve this problem. In other words, we replace the intractable conditional distributions of the terms in (21) with Gaussian distributions and ignore the terms that are irrelevant to $G(\cdot, \cdot)$. This leads to the following data-driven learning objective for $G(\cdot, \cdot)$, denoted by \mathcal{L}_G :

$$\mathcal{L}_G \triangleq \mathbb{E}_{\bar{\mathbf{x}} \sim p_Q(\bar{\mathbf{x}}|\mathbf{x}), \mathbf{x} \in \mathcal{T}} \left[\|\mathbf{x} - \hat{\mathbf{x}}\|^2 + \beta \|F(\mathbf{x}) - F(\hat{\mathbf{x}})\|^2 \right]. \quad (22)$$

E. Learning Algorithm

We now elaborate on the design of the learning algorithm for the proposed DRL framework. In the formulation of the problem proposed thus far, the learning objectives for $G(\cdot, \cdot)$ and $Q(\cdot, \mathbf{n})$ are not mutually exclusive. Given the RFF \mathbf{z} , improving the quality of the signal reconstruction requires that the other input to $G(\cdot, \cdot)$, i.e., the signal background $\bar{\mathbf{x}}$, contains as much information from the original signal as possible. This is also a part of the learning objective of $Q(\cdot, \mathbf{n})$, i.e., \mathcal{L}_v in (20). Moreover, driven by the experimental results, we find that jointly training $G(\cdot, \cdot)$ and $Q(\cdot, \mathbf{n})$ can provide less signal reconstruction error and hence higher quality synthesized signals. Based on the above considerations, we merge the learning of $G(\cdot, \cdot)$ and $Q(\cdot, \mathbf{n})$ into one step, referred to as the Q/G-step.

On the other hand, the learning of $F(\cdot)$ requires only the raw signals and the corresponding augmented signals generated by $Q(\cdot, \mathbf{n})$ and $G(\cdot, \cdot)$. Additionally, as a discriminator, $F(\cdot)$ should be made independent of the others. We therefore implement the learning of $F(\cdot)$ in a single step, referred to as the F-step.

In summary, the learning algorithm of the proposed DRL framework is composed of the following two steps.

Q/G-step: Fixing $F(\cdot)$, we optimize $Q(\cdot, \mathbf{n})$ and $G(\cdot, \cdot)$ to learn to factorize and reconstruct the received signals in the training data set, as depicted in Fig. 4. By applying the gradient descent algorithm, $Q(\cdot, \mathbf{n})$ and $G(\cdot, \cdot)$ are updated as follows

$$Q \leftarrow Q - \eta \nabla_Q (\mathcal{L}_Q + \mathcal{L}_G), \quad G \leftarrow G - \eta \nabla_G (\mathcal{L}_Q + \mathcal{L}_G), \quad (23)$$

TABLE I
THE BASIC STRUCTURE OF THE RFF EXTRACTOR $F(\cdot)$

HyperParams: Image width s , complexity L		
Input: Signal $\mathbf{x} \in \mathbb{C}^M \rightarrow$ Image $\mathbf{I} \in \mathbb{R}^{2 \times \frac{M}{S} \times S}$		
Convolution layers		
Layers	Parameters	Activation
i	Filters: $2^{i-1}L \times 3 \times 3$ Stride: $2 - (i \bmod 2)$ Padding: 1	BN + LReLU _(0.2)
Applying convolutional layers until the output is smaller than the filter size.		
Output: FC(output of convolutional layers, output dimension)		

where $\eta > 0$ is the learning rate.

F-step: Fixing $G(\cdot, \cdot)$ and $Q(\cdot, \mathbf{n})$, we optimize $F(\cdot)$ to learn to extract identical RFFs from the raw signals and the corresponding augmented signals with different backgrounds, as presented in Fig. 2. Similar to (23), $F(\cdot)$ and the auxiliary classifier are updated as

$$F \leftarrow F - \eta \nabla_F(\mathcal{L}_F), \quad \mathbf{W} \leftarrow \mathbf{W} - \eta \nabla_{\mathbf{W}}(\mathcal{L}_F), \quad (24)$$

respectively.

The training of the proposed DRL framework is performed by implementing these two steps iteratively. The corresponding training algorithm is also described in Algorithm 1.

As the learning progresses, the RFF extractor $F(\cdot)$ is gradually trained to extract only device-relevant information. Learning the background extractor $Q(\cdot, \cdot)$ relies on $F(\cdot)$, and therefore also benefits from the improvement of $F(\cdot)$. The improvement of $Q(\cdot, \cdot)$ then leads to clearer signal backgrounds, containing less device-relevant information and providing higher quality disentangled representations. With higher quality signal representations, the synthetic signal generator can create more realistic signals that only swap the background with minimal leakage of device-relevant information. The more realistic the augmented signals, the better $F(\cdot)$ can be generalized to real-world unknown channel statistics.

F. Implementation Details

We propose to adopt CNNs to learn the representations. Unless otherwise specified, the implementation of the proposed DRL framework uses the following settings:

- **Preprocessing.** All input signals to the neural networks are first normalized to $[-1, 1]$ and then converted into images. More specifically, we convert each complex input signal to a

Algorithm 1 Proposed DRL for RFF Extraction

Input: Training data set \mathcal{T} , Batch size B .

Output: F^* , Q^* , and, G^* .

Hyperparam: Learning rate η , radius δ , coefficients λ , α and β .

repeat

 # **Q/G-step:**

 Draw batch data $(\mathbf{x}^{(i)}, \mathbf{y}^{(i)})$ from \mathcal{T} , sample $\mathbf{n}^{(i)} \sim \mathcal{N}(0, \mathbf{I})$;

 Compute $\bar{\mathbf{x}}^{(i)} = Q(\mathbf{x}^{(i)}, \mathbf{n}^{(i)})$, $\mathbf{z}^{(i)} = F(\mathbf{x}^{(i)})$;

 Compute $\mathcal{L}_Q = \mathcal{L}_v + \lambda \mathcal{L}_p$ according to (16)-(20);

 Compute $\hat{\mathbf{x}}^{(i)} = G(\mathbf{z}^{(i)}, \bar{\mathbf{x}}^{(i)})$;

 Compute \mathcal{L}_G according to (22);

 Update $Q \leftarrow Q - \eta \nabla_Q (\mathcal{L}_Q + \mathcal{L}_G)$, $G \leftarrow G - \eta \nabla_G (\mathcal{L}_Q + \mathcal{L}_G)$;

 # **F-step:**

 Draw another batch $(\mathbf{x}^{(j)}, \mathbf{y}^{(j)})$ from \mathcal{T} , sample $\mathbf{n}^{(j)} \sim \mathcal{N}(0, \mathbf{I})$;

 Compute $\bar{\mathbf{x}}^{(j)} = Q(\mathbf{x}^{(j)}, \mathbf{n}^{(j)})$;

 Swap the background and generate $\hat{\mathbf{x}}^{(i,j)} = G(\mathbf{z}^{(i)}, \bar{\mathbf{x}}^{(j)})$;

 Compute \mathcal{L}_F according to (13);

 Update $F \leftarrow F - \eta \nabla_F \mathcal{L}_F$, $\mathbf{W} \leftarrow \mathbf{W} - \eta \nabla_{\mathbf{W}} \mathcal{L}_{\text{RFF}}$;

until convergence

return F , Q , and G .

2-channel real-valued image of dimension $(2 \times \frac{M}{S} \times S)$, where M is the dimension of the input, and S is width of the resultant image. The first channel of the image is the real part of the signal and the second is the imaginary part. For instance, in the experiments of this paper, we convert the 1280-length signals into the images of dimension $(2 \times 16 \times 80)$. This conversion preserves the periodic information on the image spatial correlation, facilitating the subsequent learning by the convolutional layers.

- **The RFF extractor.** The RFF extractor, $F(\cdot)$, implemented using the basic convolutional neural network (BCNN) adopted in [13], as shown in Table I. We employ a small filter with few parameters in the convolutional layers to achieve a large effective receptive field. Batch normalization and LeakyReLU(0.2) are adopted for training stability and network non-linearity, respectively. We continue applying convolutional layers until the output feature maps are smaller than the filter size, i.e., (3×3) , and final output the representations are computed by a fully connected layer. The hyper-parameter L controls the network complexity.
- **The background extractor & the signal generator.** For domain preservation, the background signal extractor $Q(\cdot, \mathbf{n})$ and the signal generator $G(\cdot, \cdot)$ in this work are both implemented

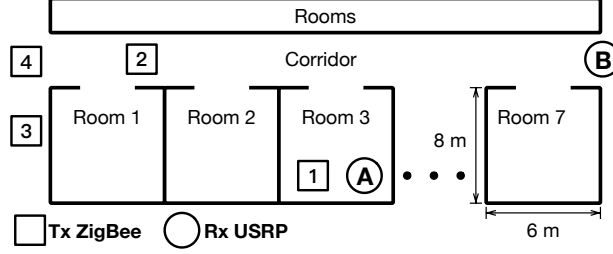


Fig. 5. The layout of device positions in the testbed.

using a U-net [48]. The U-net is a specific type of CNN with symmetrical shortcuts designed for image-domain-preserving processing and is widely used in medical image processing and image segmentation. The detailed structure of $Q(\cdot, \mathbf{n})$ and $G(\cdot, \cdot)$ is discussed in Appendix A.

- **Optimizer.** All of the neural networks are trained using Adam [41] with learning rate $\eta = 0.001$ and parameters $\beta_1 = 0.9$, and $\beta_2 = 0.999$.
- **Hyper-parameters.** We find that the performance of the proposed DRL framework is not sensitive to the choices of the hyper-parameters. The proposed approach works well in the tests sets of our experiments for a wide range of the parameters: $\lambda \in [0.3, 0.6]$, $\alpha \in [5, 30]$, $\beta \in [8, 50]$. In the results depicted in the next section, we set the hyper-parameters as $\lambda = 0.5$, $\alpha = 10$, and $\beta = 10$. We also set the hyper-parameter in the information constraint in (14) to be 0, i.e., $\epsilon = 0$. As in the previous work [25], we set the radius of the HP to be $\delta = 10$.

The implementation details are also available online in our Github at [49]. All the source codes are implemented in PyTorch using our own DL research toolbox **MarvelToolbox** [50].

IV. EXPERIMENTAL EVALUATION

In this section, we evaluate the effectiveness of the proposed DRL framework using data collected from a real-world testbed. We compare the performance of the proposed DR-RFF extractor with that of the existing ML RFF extractor (denoted by ML-RFF) and the ML RFF extractor trained with handcrafted DA (denoted by DA-RFF). The experiments consist of three parts: 1) Performance comparisons for different open test sets which contain both the unknown devices and the unknown multi-path channels; 2) Performance comparison for different signal-to-noise ratios (SNRs); 3) Learning curve comparisons for overfitting evaluation.

A. Experimental Setup

a) *Dataset*: We exploit the signals transmitted from 59 TI CC2530 ZigBee devices and collected via a USRP N210 receiver in different positions. All ZigBee devices operate at 2.4 GHz with a maximum transmit power of 19 dBm. The sampling rate of the receiver is 10 Msample/s and thus each preamble signal \mathbf{x} contains $M = 1280$ sample points.

To evaluate the effectiveness of the proposed DRL framework under the unknown channel statistics, we collect the required datasets from the different positions, shown in Fig. 5. We denote the signals, collected from the ZigBee devices transmitting at position 1 and received at position A as **TX1-RXA**. Analogously, we list all the collecting positions adopted in the experiments:

- **TX1-RXA**: the ZigBee devices are close to the receiver at a range of $0.3 \sim 2$ meters;
- **TX2-RXA**: the ZigBee devices are 10 meters away from the receiver without a direct propagation path;
- **TX3-RXA**: the ZigBee devices are 20 meters away from the receiver without a direct propagation path;
- **TX4-RXB**: the ZigBee devices are 40 meters away from the receiver with a direct propagation path.

Table II provides further details about the data sets used in this paper. The training and validation sets contain signals from 45 ZigBee devices under TX1-RXA collected in 2016. The test sets can be divided into types according to whether they have the same propagation environment with the training set:

- **T1-T3** are test sets collected in the same propagation environment as the training set, and the algorithm performance is evaluated based on whether 1) the test sets contain known devices and 2) they experience device aging. The devices considered in T1 and T3 experienced device aging since they operated continuously for over 18 months.
- **M1-M3** are collected from five unknown devices and three types of unknown wireless channels in order of classification difficulty from easy to hard. The easiest one, i.e., M1, contains only a single unknown multi-path fading channel, while M3 has three types of unknown channels and is the most challenging considered case for open-set classification.

Since the test sets are collected with different positions and running times, the main factors that affect the identification performance are the unknown multi-path fading channels and device aging.

TABLE II
DATASET FOR EVALUATION

Datasets	Device IDs	Collection Environment		Properties		
		Positions	Dates	Unknown Device	Device Aging	Multi-path
Training set	1-45	TX1-RXA	Jun. 2016	-	-	×
Validation set				×	×	×
Test set: T1	1-45	TX1-RXA	Jan. 2018, Feb. 2018	×	✓	×
Test set: T2	46-54		Jun. 2016	✓	×	×
Test set: T3			Jan. 2018, Feb. 2018	✓	✓	×
Test set: M1	55-59	TX2-RXA	Apr. 2018	✓	×	✓
Test set: M2		TX2-RXA, TX3-RXA		✓	×	✓
Test set: M3		TX2-RXA, TX3-RXA, TX4-RXB		✓	×	✓

b) Metrics: As commonly adopted in the open-set recognition tasks [13], [26], [51], we use the receiver operating characteristic (ROC) curve, the area under the ROC curve (AUC), and the equal error rate (EER) operating point to evaluate the performance of the RFF extractors. The ROC curve depicts the trade-off between true-positive rate (TPR) and false-positive rate (FPR). To obtain the ROC curve, we compute the TPR and the FPR by traversing the verification thresholds T in (3). Given a certain T , TPR refers to the probability that signal pairs from the same device are correctly verified as the same devices by the verification system. FPR refers to the percentage of the signal pairs from the same devices that yielded false alarms by the verification system. The EER refers to the point where FNR (i.e., 1-TPR) and FPR are equal.

A larger AUC and a lower EER indicate a more discriminative RFF has been, indicating that fewer false negatives and fewer false positives can be simultaneously achieved.

c) Baselines and the Proposed DR-RFFs: We consider four types of baselines, also shown in Table III:

- **ML-RFF:** A typical RFF extractor trained using MLE, without any data augmentation [13];
- **DA-RFF:** ML-RFF with DA that adds handcrafted white Gaussian noise (SNR: 5 ~ 30 dB) to the training data;
- **DR-RFF-A:** An RFF extractor trained by the proposed DRL framework, without any handcrafted DA;
- **DR-RFF-B:** An RFF extractor trained by the proposed DRL framework, with handcrafted DA that adds white Gaussian noise (SNR: 5 ~ 30 dB) to the training data.

Unless otherwise specified, all the baseline approaches use the same network structure (see

TABLE III
BASELINES RFF EXTRACTORS AND THE PROPOSED DR-RFF

Baselines	Training Methods	Data Augmentation	The Conditional Distribution in (4): $p_{\mathbf{W}}(\mathbf{y} F(\mathbf{x}))$		# Parameters
			RFF extractor	Auxiliary Classifier	
ML-RFF	MLE	N/A	BCNN [13] ($L = 18$)	Softmax with HP [13] ($\delta = 10$)	$\approx 7 \text{ M}$
DA-RFF		AWGN (SNR: 5 ~ 30 dB)			
DR-RFF-A [†]	DRL [†]	N/A		Softmax	
				Softmax with HP [13] ($\delta = 10$)	
DR-RFF-B [†]		AWGN (SNR: 5 ~ 30 dB)		Softmax	
				Softmax with HP [13] ($\delta = 10$)	

[†] Proposed in this paper.

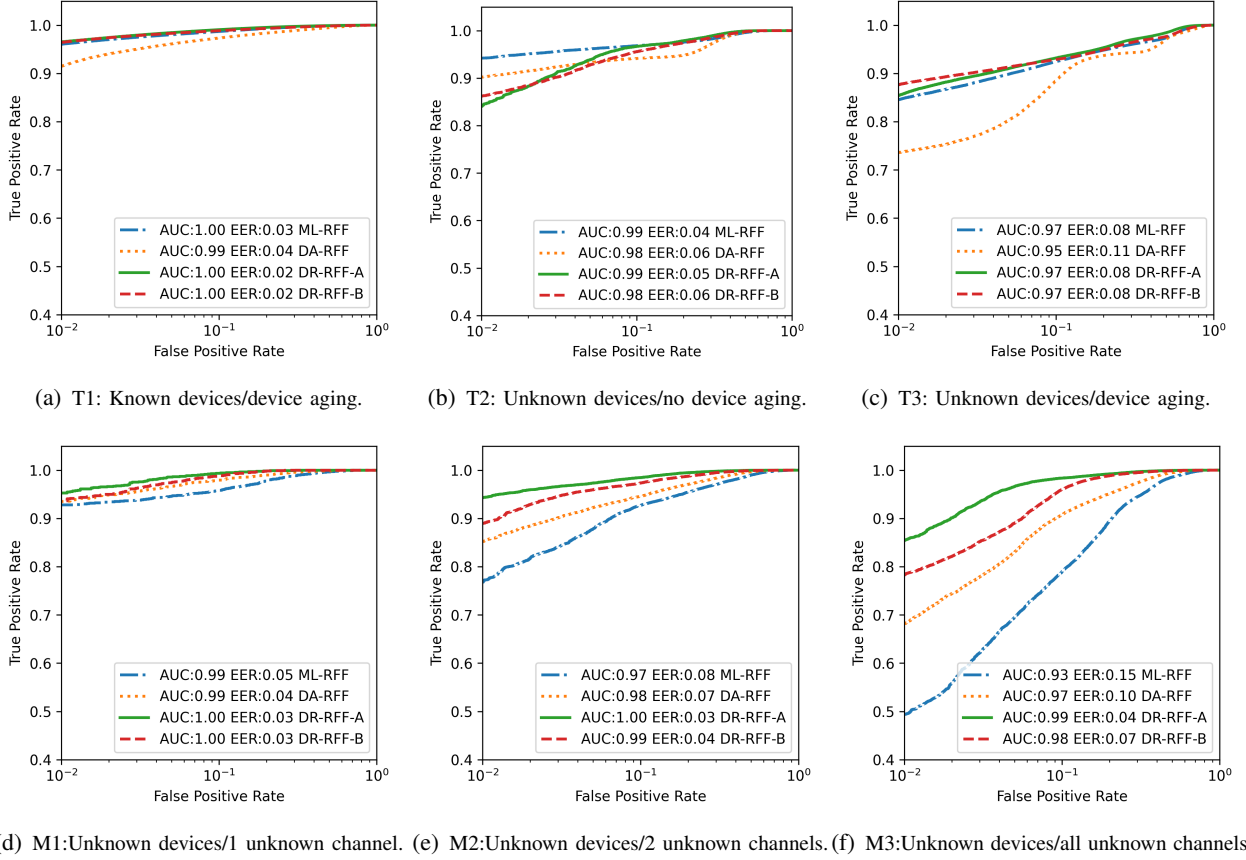


Fig. 6. ROC curves of different methods under different open set settings (SNR = 30 dB). The test sets, T1-T3, are collected at the same position as the training set, while M1-M3 are collected from unknown devices at unknown positions.

Table I) with the same complexity setting of $L = 18$, and all apply the HP operation to the RFF (in Section III.B). ML-RFF and DA-RFF are both trained by Adam with the same setting as the proposed DR-RFF-A/B.

TABLE IV
ROC COMPARISON OF DIFFERENT METHODS

Baselines	T2		T3		M1		M2		M3	
	AUC	EER	AUC	EER	AUC	EER	AUC	EER	AUC	EER
ML-RFF	0.9884	0.0406	0.9682	0.0827	0.9877	0.0530	0.9711	0.0831	0.9349	0.1519
DA-RFF	0.9803	0.0635	0.9520	0.1064	0.9933	0.0390	0.9826	0.0671	0.9671	0.0960
DR-RFF-A w/o HP [†]	0.9914	0.0525	0.9683	0.0783	0.9743	0.0849	0.9632	0.1001	0.9507	0.1372
DR-RFF-A [†]	0.9865	0.0548	0.9741	0.0763	0.9973	0.0272	0.9953	0.0326	0.9919	0.0417
DR-RFF-B w/o HP [†]	0.9845	0.0777	0.9671	0.0736	0.9887	0.0512	0.9682	0.0926	0.9715	0.0835
DR-RFF-B [†]	0.9846	0.0622	0.9709	0.0771	0.9960	0.0342	0.9911	0.0434	0.9840	0.0716

[†] Proposed in this paper.

B. Performance Under Unknown Devices & Channel Statistic

In order to investigate the effectiveness of the proposed DRL framework, we plot the ROC curves in Fig. 6 comparing the performance of the RFFs trained under our proposed framework against the baseline algorithms under different open-set settings. We also compare the AUC and the EER in Table IV.

a) Power of Disentangled Representation Learning: Overall, the RFF extractors trained by the proposed DRL framework (DR-RFF-A, DR-RFF-B) achieve satisfactory performance for consistent propagation conditions and outperform the conventional methods (ML-RFF, DA-RFF) for the test sets with unknown collection environments. These results verify that the RFFs extracted by the proposed approach are more channel-invariant than for the others. Even under the most challenging test set, i.e., M3 in Fig. 6(f), which contains all three types of unknown channel statistics, the proposed DR-RFF-A trained only by the proposed DRL framework can still preserve AUC over 0.99. On the other hand, although the conventional methods can perform well with known positions, their performance degrades dramatically under the difficult setting of M3. These performance degradations result from the overfitting of the channel statistics in the training set or mismatched prior distributions between the DA and the real-world situations. With the data-driven DRL, these drawbacks can to some extent be remedied. These results demonstrate the superiority of the proposed DRL framework for robust RFF extraction with unknown channels.

b) Necessity of Hypersphere Projection: To verify the necessity of the HP operation (6) in the proposed DRL framework, we compare the proposed methods (DR-RFF-A, DR-RFF-B) with their non-HP versions (DR-RFF-A w/o HP, DR-RFF-B w/o HP). We find that the DR-

RFFs with HP outperform DR-RFFs without HP for unknown channels, as evidenced by both the AUC and EER values in Table IV. We suggest that the underlying reason is the incomplete disentanglement caused by the non-HP methods. In other words, the RFFs obtained by the non-HP extractor are not discriminative enough to rule out the background information from the input signals. Thus the background extractor is unable to effectively extract the device-irrelevant information to ensure low error reconstruction. This incomplete disentanglement leads to inaccurate background swapping, which potentially reduces the generalizability of the RFF extractor to unknown channel statistics.

c) Impact of Handcrafted Data Augmentation: To further investigate the impact of using DA, we compare the performance between the model trained with DA (i.e., DA-RFF) and without DA (i.e., ML-RFF). We discover that using the hand-crafted DA technique can improve the generalizability of RFFs to unknown channels at the cost of discriminative ability (see Fig. 6(c)). However, these performance gains are still limited (see Fig. 6(f)). This suggests that the DA techniques can indeed reduce overfitting to the channel statistics in the training set. Indeed, without any prior knowledge about the real-world channels, some channel-invariant features are distorted by the DA. A similar phenomenon also appears in the proposed DRL method with DA (i.e., DR-RFF-B). For high SNR scenarios, e.g., SNR = 30 dB, DR-RFF-B produces some degradation in performance for unknown channels (see Fig. 6(d) to Fig. 6(f)). However, this feature distortion phenomenon is relieved by the proposed DRL framework. In the next section, we will demonstrate that this performance degradation arising from DA is offset by the performance gain of the proposed DRL framework, especially for low SNR scenarios.

C. Performance versus SNR

Next, we investigate the robustness of the proposed DR-RFFs with respect to the noise. We consider SNRs from 5 to 30 dB for all the test sets and the results are presented in Fig. 7. As before, DA improves the robustness by sacrificing some of the discrimination performance of the RFFs. However, we find that the proposed DRL framework can provide a better trade-off between the robustness and the discrimination performance than MLE when applying DA. By jointly using the proposed DRL framework and the DA, DR-RFF-B can still preserve performance even for the lowest SNR situations in almost all test sets. Note that this robustness is obtained at the cost of only minimal performance loss for high SNR situations (compared with DR-RFF-A in Fig. 7).

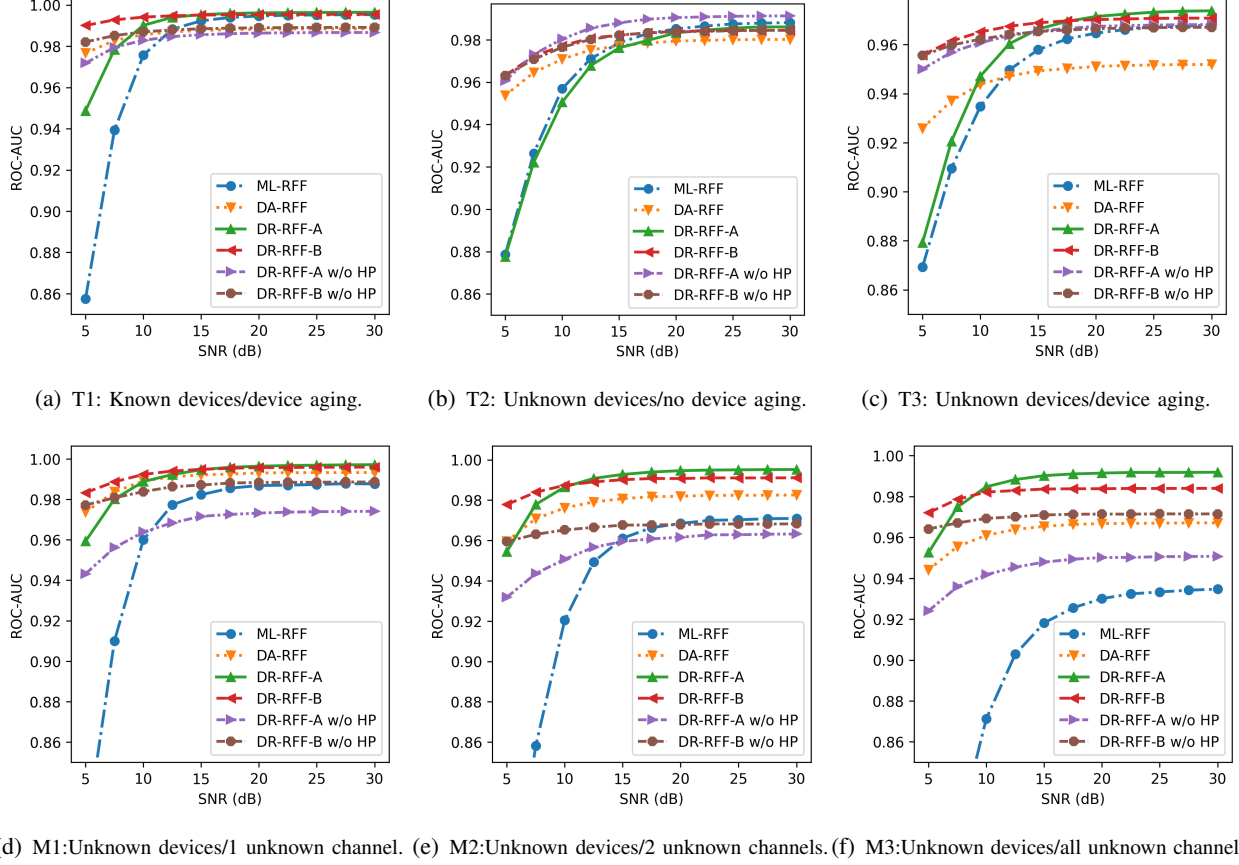


Fig. 7. SNR-AUC curves of different methods under different open set settings. The test sets, T1-3, are collected at the same position as the training set, while M1-3 are collected from unknown devices at unknown positions.

Among the conventional methods, ML-RFF has the worst robustness, which degrades its performance dramatically for all test sets when $\text{SNR} < 15$ dB. This indicates that the features used in ML-RFF are more sensitive to the noises than the others. Despite the fact that DA significantly improves the robustness of the conventional method, there still exists a large gap between DA-RFF and the proposed DR-RFFs, especially for the most challenging test set M3, as shown in Fig. 7(f).

For the non-HP methods, i.e., DR-RFF-A w/o HP and DR-RFF-B w/o HP in Fig. 7, the weakened disentanglement makes it difficult for these schemes to learn to rule out the background information from training data, thus leading to overfitting. For instance, DR-RFF-A w/o HP can only perform well under test set T2 in Fig. 7(b). This implies that DR-RFF-A w/o HP is overfitting the non-device-aging channel in the training data and significantly losing its generalizability to the other channels.

These results demonstrate the superiority of the proposed DRL framework and again highlight

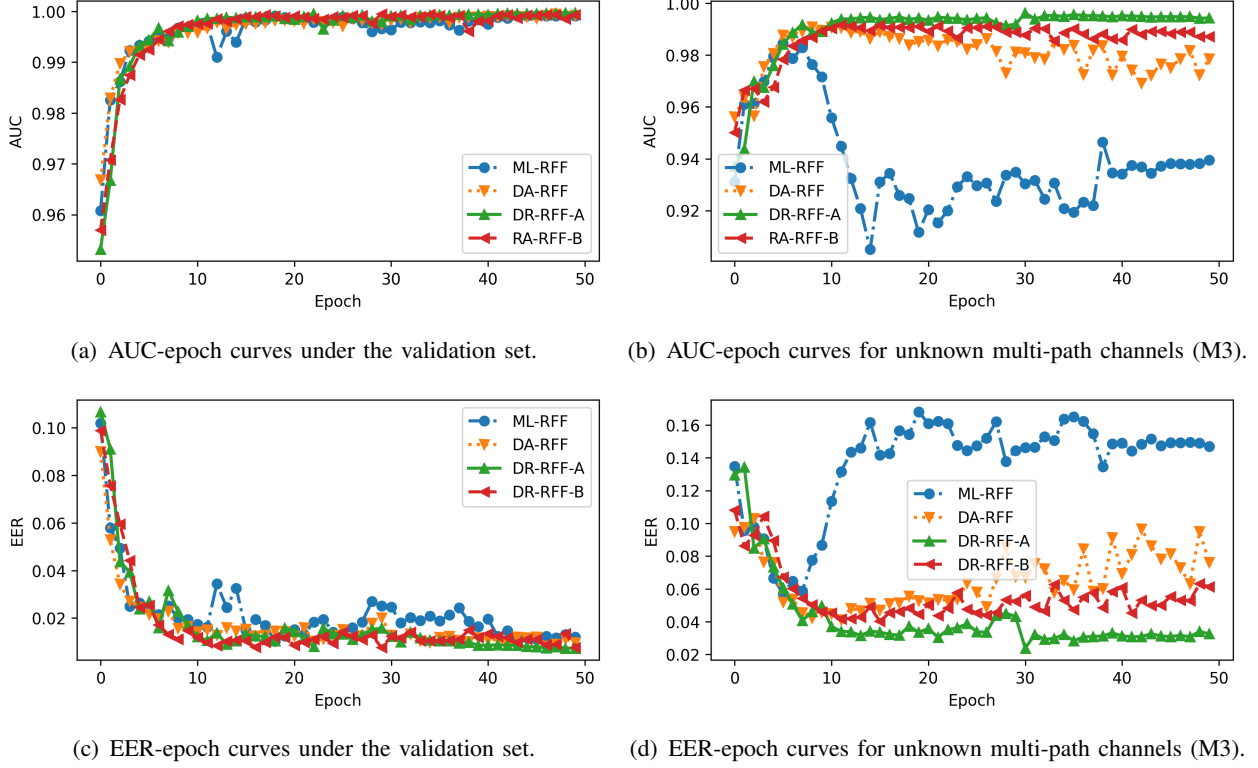


Fig. 8. Learning curves of different methods under the validation and open test sets (SNR = 30 dB).

the need for HP. Also, they indicate that the hand-crafted DA is a “blessing” rather than a “curse” to the proposed DRL framework.

D. Comparison of Learning Curves

Finally, we compare the proposed DR-RFFs with the conventional methods from the perspective of the learning process. We record the performance of the baseline approaches and the proposed DR-RFFs in each training epoch and then plot in Fig. 8. The learning curves with the number of training epochs on the horizontal axis and either AUC or EER on the vertical axis.

Fig. 8(a) and Fig. 8(c) are the learning curves for the validation set. Since the validation set shares the same data distribution with the training set, the performance achieved here indicates the progress of learning the training set. Fig. 8(b) and Fig. 8(d) are the learning curves for the test set with three types of unknown channels, which reveals potential overfitting to the channel statistics embedded in the training set.

The learning curves in Fig. 8(a) and Fig. 8(c) show that all methods provide a good fit to the training set and near-perfect classification performance under the validation set. However,

for the test set with unknown channel statistics in Fig. 8(b) and Fig. 8(d), the overfitting of the conventional methods occurs in the early stages of training, e.g., the eighth epoch for ML-RFF. Although DA can to some extent alleviate the overfitting phenomenon, the degree of overfitting increases as the learning process continues.

By contrast, overfitting in DR-RFF-A is suppressed by the proposed DRL framework. Even towards the end of the training, DR-RFF-A is adaptive to unknown channel statistics and performs well. Regarding DR-RFF-B, which is jointly trained by both DA and the proposed DRL framework, its degree of overfitting is between DA-RFF and DR-RFF-A. These results again confirm that applying the proposed DRL framework can effectively avoid overfitting some channel statistics embedded in the training set and counteract the performance degradation brought by DA.

V. CONCLUSIONS

In this paper, we proposed a novel DRL framework for improving the robustness and generalizability of DL-based RFF to unknown channel statistics. The DL-RFFs trained by adopting MLE tend to overfit the non-representative channel statistics in the training set and thus lose their generalizability to unknown channels. To address this problem, we proposed a novel DRL framework that factors the signal into two disjoint parts: a device-relevant representation (i.e., the RFF) and a device-irrelevant representation (i.e., the signal background), and can generate signals based on this decomposition. Even when all signals in the training set are collected in a simple propagation environment, distinctions in their signal background can still exist. With the help of the proposed DRL framework, we shuffle the signal backgrounds in the training set and mimic transmissions from different types of environments without collecting additional data. In this way, the RFF extractor trained with the proposed framework is encouraged to extract the channel-invariant features as the RFFs. Our experimental results showed that the proposed framework significantly improved the discrimination performance of RFFs under unknown multipath fading channels and provided a better trade-off between robustness and performance than the conventional methods.

APPENDIX A

THE DETAILED STRUCTURES OF $Q(\cdot, \mathbf{n})$ AND $G(\cdot, \cdot)$

In this section, we introduce the detailed structure of the background signal extractor $Q(\cdot, \mathbf{n})$ and the signal generator $G(\cdot, \cdot)$. Since $Q(\cdot, \mathbf{n})$ and $G(\cdot, \cdot)$ in this work are both based on U-net [48], we first introduce the basic modules of U-net [48] and then elaborate on the design of $Q(\cdot, \mathbf{n})$ and $G(\cdot, \cdot)$.

a) *The Basic Modules of U-net:* As shown in Table V, U-net consists of three basic modules: *DoubleConv*, *DownConv*, *UpConv*, and *Catenate*. They are described as follows.

- *DoubleConv*, contains two convolutional layers with C_{out} kernel size of 3×3 , 1 padding, 1 stride (denoted by $\text{Conv2D}(C_{\text{out}}, 3 \times 3, 1, 1)$) and the BN+ReLU activation. It takes image $\mathbf{I} \in \mathbb{R}^{C_{\text{in}} \times W \times H}$ as input, and outputs an image with the same weight and height, i.e., $\mathbf{I} \in \mathbb{R}^{C_{\text{out}} \times W \times H}$, where C_{in} , H , and W represent the number of channels, the weight, and the height of the image, respectively.
- *DownConv*. Down-sampling module, contains one max pooling layer and one *DoubleConv* module, takes image $\mathbf{I} \in \mathbb{R}^{C_{\text{in}} \times W \times H}$ as input, and outputs an image with half the weight and height of the input, i.e., $\mathbf{I} \in \mathbb{R}^{C_{\text{out}} \times \frac{W}{2} \times \frac{H}{2}}$.
- *UpConv*. Up-sampling module, contains one up-sampling layer and two convolutional layers, takes image $\mathbf{I} \in \mathbb{R}^{C_{\text{in}} \times W \times H}$ as input, and outputs an image with twice the weight and height of the input, i.e., $\mathbf{I} \in \mathbb{R}^{C_{\text{out}} \times \frac{W}{2} \times \frac{H}{2}}$.
- *Catenate*. This module merges two images along the channel dimension of the images.

b) *Structure of $Q(\cdot, \mathbf{n})$ and $G(\cdot, \cdot)$:* As presented in Table VI, both $Q(\cdot, \mathbf{n})$ and $G(\cdot, \cdot)$ contain down-sampling and up-sampling phases. The down-sampling phase consists of one *DoubleConv* module and four down-sampling modules. The up-sampling phase contains four up-sampling modules, one convolutional layer, and four layers for concatenating the outputs from the up-sampling and the down-sampling phases. These concatenated layers provide shortcuts that enable the input images to skip the NN processing at different levels of abstraction, thus leading to the property of image domain preservation. The only difference between $Q(\cdot, \mathbf{n})$ and $G(\cdot, \cdot)$ are the layers in the middle. As shown in Table VI, $Q(\cdot, \mathbf{n})$ adds random noise to the latent image, i.e., \mathbf{I}_5 , while $G(\cdot, \cdot)$ adds the RFF \mathbf{z} to \mathbf{I}_5 .

TABLE V
THE BASIC MODULES OF U-NET

DoubleConv (C_{out})	
HyperParams: The number of output channels C_{out}	
Input: Image $\mathbf{I} \in \mathbb{R}^{C_{in} \times W \times H}$	
Layers	Activation
1. Conv2D($C_{out}, 3 \times 3, 1, 1$)	BN + ReLU
2. Conv2D($C_{out}, 3 \times 3, 1, 1$)	BN + ReLU
Output: Image $\mathbf{I} \in \mathbb{R}^{C_{out} \times W \times H}$	
DownConv (C_{out})	
HyperParams: The number of output channels C_{out}	
Input: Image $\mathbf{I} \in \mathbb{R}^{C_{in} \times W \times H}$	
Layers	
1. MaxPool2d(2)	
2. DoubleConv(C_{out})	
Output: Image $\mathbf{I} \in \mathbb{R}^{C_{out} \times \frac{W}{2} \times \frac{H}{2}}$	
UpConv (C_{out})	
HyperParams: The number of output channels C_{out}	
Input: Image $\mathbf{I} \in \mathbb{R}^{C_{in} \times W \times H}$	
Layers	Activation
1. Upsample(2)	
2. Conv2D($C_{in}/2, 3 \times 3, 1, 1$)	BN + ReLU
3. Conv2D($C_{out}, 3 \times 3, 1, 1$)	BN + ReLU
Output: Image $\mathbf{I} \in \mathbb{R}^{C_{out} \times 2W \times 2H}$	
Catenate	
Catenating two images along the dimension of channels.	
Input: Images $\mathbf{I}_1 \in \mathbb{R}^{C_1 \times W \times H}$, and $\mathbf{I}_2 \in \mathbb{R}^{C_2 \times W \times H}$	
Output: Image $\mathbf{I} \in \mathbb{R}^{(C_1+C_2) \times W \times H}$	

TABLE VI
THE STRUCTURE OF $Q(\cdot, \mathbf{n})$ OR $G(\cdot, \cdot)$

Input: Signal $\mathbf{x} \in \mathbb{C}^M \rightarrow$ Image $\mathbf{I} \in \mathbb{R}^{2 \times \frac{M}{S} \times S}$			
Layers	Inputs \rightarrow	Modules \rightarrow	Outputs
# Down-sampling phase:			
1	\mathbf{I}	DoubleConv(64)	\mathbf{I}_1
2	\mathbf{I}_1	DownConv(128)	\mathbf{I}_2
3	\mathbf{I}_2	DownConv(256)	\mathbf{I}_3
4	\mathbf{I}_3	DownConv(512)	\mathbf{I}_4
5	\mathbf{I}_4	DownConv(512)	\mathbf{I}_5
# For $Q(\cdot, \mathbf{n})$: Adding randomness with $\mathbf{n} \sim \mathcal{N}(\mathbf{0}, \mathbf{I})$			
6	\mathbf{I}_5 and \mathbf{n}	$\mathbf{I}_5^* = \mathbf{I}_5 + \mathbf{n}$	\mathbf{I}_5^*
# For $G(\cdot, \cdot)$: Adding RFF			
6-1	\mathbf{z}	FC(the shape of \mathbf{I}_5)	\mathbf{I}_z
6-2	\mathbf{I}_5 and \mathbf{I}_z	$\mathbf{I}_5^* = \mathbf{I}_5 + \mathbf{I}_z$	\mathbf{I}_5^*
# Up-sampling phase:			
7	\mathbf{I}_5^*	UpConv(256)	\mathbf{I}_4'
8	\mathbf{I}_4 and \mathbf{I}_4'	Catenate	\mathbf{I}_4^*
9	\mathbf{I}_4^*	UpConv(128)	\mathbf{I}_3'
10	\mathbf{I}_3 and \mathbf{I}_3'	Catenate	\mathbf{I}_3^*
11	\mathbf{I}_3^*	UpConv(64)	\mathbf{I}_2'
12	\mathbf{I}_2 and \mathbf{I}_2'	Catenate	\mathbf{I}_2^*
13	\mathbf{I}_2^*	UpConv(64)	\mathbf{I}_1'
14	\mathbf{I}_1 and \mathbf{I}_1'	Catenate	\mathbf{I}_1^*
15	\mathbf{I}_1^*	Conv2D(2, $1 \times 1, 1, 1$)	\mathbf{I}_{out}
Output: Image $\mathbf{I}_{out} \in \mathbb{R}^{2 \times \frac{M}{S} \times S} \rightarrow$ Signal $\mathbf{x}_{out} \in \mathbb{C}^M$			

REFERENCES

- [1] L. Peng, J. Zhang, M. Liu, and A. Hu, "Deep learning based RF fingerprint identification using differential constellation trace figure," *IEEE Trans. Veh. Technol.*, vol. 69, no. 1, pp. 1091–1095, Oct. 2019.
- [2] W. Wang, Z. Sun, S. Piao, B. Zhu, and K. Ren, "Wireless physical-layer identification: Modeling and validation," *IEEE Trans. Inf. Forensics Security*, vol. 11, no. 9, pp. 2091–2106, Sep. 2016.
- [3] W. Hou, X. Wang, J.-Y. Chouinard, and A. Refaey, "Physical layer authentication for mobile systems with time-varying carrier frequency offsets," *IEEE Trans. Commun.*, vol. 62, no. 5, pp. 1658–1667, Apr. 2014.
- [4] V. Brik, S. Banerjee, M. Gruteser, and S. Oh, "Wireless device identification with radiometric signatures," in *Proc. 14th ACM Int. Conf. Mobile Comput. Netw. (MobiCom)*, New York, NY, USA, Sep. 2008, pp. 116–127.
- [5] J. Hall, M. Barbeau, and E. Kranakis, "Enhancing intrusion detection in wireless networks using radio frequency fingerprinting," in *Proc. Third IASTED Int. Conf. Commun. Internet Inf. Technol. Eng.*, Jan. 2004, pp. 201–206.
- [6] D. A. Knox and T. Kunz, "AGC-based RF fingerprints in wireless sensor networks for authentication," in *Proc. IEEE Int. Symp. WoWMoM, Montreal, QC, Canada*, Aug. 2010, pp. 1–6.
- [7] X. Chen, D. W. K. Ng, W. Yu, E. G. Larsson, N. Al-Dhahir, and R. Schober, "Massive access for 5G and beyond," *IEEE J. Sel. Areas Commun.*, vol. 39, no. 3, pp. 615–637, Sep. 2020.
- [8] Y. Sun, W. Xu, L. Liang, N. Wang, G. Y. Li, and X. You, "A lightweight deep network for efficient CSI feedback in massive MIMO systems," *IEEE Commun. Lett.*, vol. 10, no. 8, pp. 1840–1844, May 2021.

- [9] S. Zhang, J. Xu, W. Xu, N. Wang, D. W. K. Ng, and X. You, "Data augmentation empowered neural precoding for multiuser MIMO with MMSE model," *IEEE Commun. Lett.*, early access, Mar. 2022.
- [10] Z. Yin, W. Xu, R. Xie, S. Zhang, D. W. K. Ng, and X. You, "Deep CSI compression for massive MIMO: A self-information model-driven neural network," *IEEE Trans. Wireless Commun.*, May. 2022, early access.
- [11] K. Merchant, S. Revay, G. Stantchev, and B. Noursain, "Deep learning for RF device fingerprinting in cognitive communication networks," *IEEE J. Sel. Top. Signal Process.*, vol. 12, no. 1, pp. 160–167, Jan. 2018.
- [12] J. Yu, A. Hu, G. Li, and L. Peng, "A robust RF fingerprinting approach using multisampling convolutional neural network," *IEEE Internet Things J.*, vol. 6, no. 4, pp. 6786–6799, Apr. 2019.
- [13] R. Xie, W. Xu, Y. Chen, J. Yu, A. Hu, D. W. K. Ng, and A. L. Swindlehurst, "A generalizable model-and-data driven approach for open-set RFF authentication," *IEEE Trans. Inf. Forensics Security*, vol. 16, pp. 4435–4450, Aug. 2021.
- [14] G. Shen, J. Zhang, A. Marshall, and J. R. Cavallaro, "Towards scalable and channel-robust radio frequency fingerprint identification for LoRa," *IEEE Transactions on Information Forensics and Security*, vol. 17, pp. 774–787, Feb. 2022.
- [15] A. Al-Shawabka, P. Pietraski, S. B. Pattar, F. Restuccia, and T. Melodia, "DeepLoRa: Fingerprinting LoRa devices at scale through deep learning and data augmentation," in *Proc. ACM Int. Symposium Mob. Ad Hoc Netw. Comput.*, Jul. 2021, pp. 251–260.
- [16] N. Soltani, K. Sankhe, J. Dy, S. Ioannidis, and K. Chowdhury, "More is better: Data augmentation for channel-resilient RF fingerprinting," *IEEE Communications Magazine*, vol. 58, no. 10, pp. 66–72, Nov. 2020.
- [17] I. Higgins, D. Amos, D. Pfau, S. Racanière, L. Matthey, D. J. Rezende, and A. Lerchner, "Towards a definition of disentangled representations," *CoRR*, vol. abs/1812.02230, Dec. 2018.
- [18] D. P. Kingma and M. Welling, "Auto-encoding variational bayes," in *Proc. Int. Conf. Learn. Representations*, Banff, AB, Canada, Apr. 2014.
- [19] X. Chen, Y. Duan, R. Houthoofd, J. Schulman, I. Sutskever, and P. Abbeel, "InfoGAN: Interpretable representation learning by information maximizing generative adversarial nets," in *Proc. Adv. Neural Inf. Process. Syst.*, Barcelona, Spain, Dec. 2016, pp. 2172–2180.
- [20] I. Higgins, L. Matthey, A. Pal, C. P. Burgess, X. Glorot, M. M. Botvinick, S. Mohamed, and A. Lerchner, "beta-VAE: Learning basic visual concepts with a constrained variational framework," in *Proc. Int. Conf. Learn. Representations*, Toulon, France, Apr. 2017.
- [21] K. M. Chen and R. Y. Chang, "A comparative study of deep-learning-based semi-supervised device-free indoor localization," in *Proc. IEEE GLOBECOM*, Madrid, Spain, Dec. 2021, pp. 1–6.
- [22] K. Choi, K. Tatwawadi, A. Grover, T. Weissman, and S. Ermon, "Neural joint source-channel coding," in *Proc. Int. Conf. Mach. Learn.*, vol. 97. PMLR, Jun. 2019, pp. 1182–1192.
- [23] Y. M. Saidutta, A. Abdi, and F. Fekri, "Joint source-channel coding over additive noise analog channels using mixture of variational autoencoders," *IEEE J. Sel. Areas Commun.*, vol. 39, no. 7, pp. 2000–2013, Jul. 2021.
- [24] J. Gong, X. Xu, and Y. Lei, "Unsupervised specific emitter identification method using radio-frequency fingerprint embedded InfoGAN," *IEEE Trans. Inf. Forensics Security*, vol. 15, pp. 2898–2913, Mar. 2020.
- [25] R. Ranjan, C. D. Castillo, and R. Chellappa, "L2-constrained softmax loss for discriminative face verification," *CoRR*, vol. abs/1703.09507, Mar. 2017.
- [26] J. Deng, J. Guo, N. Xue, and S. Zafeiriou, "Arcface: Additive angular margin loss for deep face recognition," in *Proc. IEEE Conf. Comput. Vis. Pattern Recognit.*, Jun. 2019, pp. 4690–4699.
- [27] W. Liu, Y. Wen, Z. Yu, M. Li, B. Raj, and L. Song, "Sphreface: Deep hypersphere embedding for face recognition," in *Proc. IEEE Conf. Comput. Vis. Pattern Recognit.*, Jul. 2017, pp. 212–220.
- [28] D. Barber, *Bayesian reasoning and machine learning*. Cambridge University Press, 2012.

- [29] Y. Bengio, A. Courville, and P. Vincent, "Representation learning: a review and new perspectives," *IEEE Trans. Pattern Anal. Mach. Intell.*, vol. 35, no. 8, pp. 1798–1828, Mar. 2013.
- [30] X. Liu, P. Sanchez, S. Thermos, A. Q. O’Neil, and S. A. Tsafaris, "A tutorial on learning disentangled representations in the imaging domain," *CoRR*, vol. abs/2108.12043, Aug. 2021.
- [31] R. Xie, Y. Wang, T. Xie, Y. Zhang, L. Xu, J. Lu, and Q. Wang, "Adversarial training for video disentangled representation," in *Proc. Int. Conf. Multimed. Modell.* Springer, Jan. 2019, pp. 532–543.
- [32] E. Denton and V. Birodkar, "Unsupervised learning of disentangled representations from video," in *Proc. Int. Conf. Neural Inf. Process. Syst.*, Dec. 2017, pp. 4417–4426.
- [33] J. Chou, C. Yeh, H. Lee, and L. Lee, "Multi-target voice conversion without parallel data by adversarially learning disentangled audio representations," *Proc. Interspeech*, pp. 501–505, Sep. 2018.
- [34] L. Tran, X. Yin, and X. Liu, "Disentangled representation learning GAN for pose-invariant face recognition," in *Proc. IEEE Conf. Comput. Vis. Pattern Recog.*, Jul. 2017, pp. 1415–1424.
- [35] T. Chen, S. Kornblith, M. Norouzi, and G. Hinton, "A simple framework for contrastive learning of visual representations," in *Proc. Int. Conf. Mach. Learn.* PMLR, Jul. 2020, pp. 1597–1607.
- [36] J. Mitrovic, B. McWilliams, J. C. Walker, L. H. Buesing, and C. Blundell, "Representation learning via invariant causal mechanisms," in *Proc. Int. Conf. Learn. Representations*, Virtual Event, Austria, May 2021.
- [37] D. P. Kingma, S. Mohamed, D. J. Rezende, and M. Welling, "Semi-supervised learning with deep generative models," in *Proc. Adv. Neural Inf. Process. Syst.*, Montreal, Quebec, Canada, Dec. 2014, pp. 3581–3589.
- [38] M. Bertrán *et al.*, "Adversarially learned representations for information obfuscation and inference," in *Proc. Int. Conf. Mach. Learn.*, ser. Proceedings of Machine Learning Research, Long Beach, California, USA, Jun. 2019, pp. 614–623.
- [39] D. J. MacKay and D. J. Mac Kay, *Information Theory, Inference and Learning Algorithms*. Cambridge University Press, 2003.
- [40] A. A. Alemi, I. Fischer, J. V. Dillon, and K. Murphy, "Deep variational information bottleneck," in *Proc. Int. Conf. Learn. Representations*, Toulon, France, Apr. 2017.
- [41] D. P. Kingma and J. Ba, "Adam: A method for stochastic optimization," in *Proc. Int. Conf. Learn. Representations*, Y. Bengio and Y. LeCun, Eds., San Diego, CA, USA, May 2015.
- [42] S. Boyd, S. P. Boyd, and L. Vandenberghe, *Convex optimization*. Cambridge University Press, 2004.
- [43] N. Tishby, F. C. N. Pereira, and W. Bialek, "The information bottleneck method," *CoRR*, vol. physics/0004057, Apr. 2000.
- [44] N. Tishby and N. Zaslavsky, "Deep learning and the information bottleneck principle," in *Proc. IEEE Inf. Theory Workshop*. IEEE, May 2015, pp. 1–5.
- [45] D. B. F. Agakov, "The IM algorithm: A variational approach to information maximization," *Proc. Int. Conf. Neural Inf. Process. Syst.*, vol. 16, no. 320, p. 201, Dec. 2004.
- [46] I. J. Goodfellow, J. Pouget-Abadie, M. Mirza, B. Xu, D. Warde-Farley, S. Ozair, A. C. Courville, and Y. Bengio, "Generative adversarial nets," in *Proc. Adv. Neural Inf. Process. Syst.*, Montreal, Quebec, Canada, Dec. 2014, pp. 2672–2680.
- [47] J. Donahue, P. Krähenbühl, and T. Darrell, "Adversarial feature learning," in *Proc. Int. Conf. Learn. Representations*, Toulon, France, Apr. 2017.
- [48] O. Ronneberger, P. Fischer, and T. Brox, "U-net: Convolutional networks for biomedical image segmentation," in *Proc. Int. Conf. Med. image Comput. Comput.-Assisted Intervention*. Springer, Nov. 2015, pp. 234–241.
- [49] R. Xie and W. Xu. (2021) DR-RFF. [Online]. Available: <https://github.com/xrj-com/DR-RFF>
- [50] R. Xie and W. Xu. (2020) MarvelToolbox. [Online]. Available: <https://github.com/xrj-com/marveltoolbox>
- [51] B. Danev, D. Zanetti, and S. Capkun, "On physical-layer identification of wireless devices," *ACM Comput. Surv.*, vol. 45, no. 1, pp. 1–29, Dec. 2012.